NASA Technical Memorandum 83571

Assessment of Three-Dimensional Inviscid Codes and Loss Calculations for Turbine Aerodynamic Computations

Louis A. Povinelli
Lewis Research Center
Cleveland, Ohio

Prepared for the
Twenty-ninth Annual International Gas Turbine Conference
sponsored by the American Society of Mechanical Engineers
Amsterdam, The Netherlands, June 3-7, 1984

NASA

ASSESSMENT OF THREE-DIMENSIONAL INVISCID CODES AND LOSS CALCULATIONS FOR TURBINE AERODYNAMIC COMPUTATIONS

Louis A. Povinelli
National Aeronautics and Space Administration
Lewis Research Center
Cleveland, Ohio

ABSTRACT

An assessment of several three-dimensional inviscid turbine aerodynamic computer codes and loss models used at the NASA Lewis Research Center is presented. Five flow situations are examined, for which both experimental data and computational results are available. The five flows form a basis for the evaluation of the computational procedures. It was concluded that stator flows may be calculated with a high degree of accuracy, whereas, rotor flow fields are less accurately determined. Exploitation of contouring, leaning, bowing, and sweeping will require a three-dimensional viscous analysis technique.

INTRODUCTION

The design and analysis of turbines requires increasingly more analytical sophistication. This increase in sophistication is required because turbine design is becoming more complex as newer features such as endwall contouring, and leaning, bowing, and sweeping of the vanes and blades are used. These newer design features in combination with lower blade aspect ratios will lead to more complicated flows within turbine stages. Along with those flows, there will be an increasing uncertainty in the heat transfer to the endwalls and to the vane and blade surfaces. A greater fundamental knowledge of the flow will be required for effective design, including such items as boundary layer state and location of transition, and the effect of turbulence on both transition and heat transfer. Interactions between the stator and rotor flow fields is also an important area that requires far greater understanding. The proper representation of the initial conditions entering the turbine, i.e., the effects of the combustor exit distortions, must also be understood as well as modeled. If these complex phenomena are to be modeled and computed, it will be necessary to develop three-dimensional viscous codes. A substantial amount of effort will be required for the development, assessment, refinement, and application of such codes. However, the potential returns in term of increased aerodynamic performance and improved heat transfer predictions make the effort worthwhile.

The current approach to the design and analysis of turbines is to rely on inviscid computations coupled with a boundary layer calculation and an assortment of loss correlations. By and large, turbomachinery designers have learned how to design and analyze turbines using that approach coupled with a great deal of intuitive judgement.

The scope of this paper is limited to the evaluation or assessment of the design procedure described above. For purposes of assessment, attention is focused on flow field computations using the inviscid computer codes, TSONIC, TSONIC/MERIDL (ref. 1, 2) and the Denton Code (ref. 3, 4). The results from an integral boundary layer code, BLAYER (ref. 5), as well as profile, mixing and endwall losses using Stewart's analysis (ref. 6) are also evaluated. Secondary flow losses, incidence losses, and tip clearance losses as determined from various loss correlations (ref. 7, 8) are evaluated as well. Comparisons are presented of the computed results with experimental data obtained from two-dimensional (ref. 9) and annular cascades (ref. 10, 11, 12), a large warm core turbine (ref. 13) and a small axial turbine (ref. 8). The method or approach used to carry out the assessment of the computations is presented in the following section.

METHOD/APPROACH

The approach used in this paper is to examine a number of experimental studies for which selected aerodynamic parameters have also been computed, and to arrive at conclusions regarding our current predictive capability. Five experiments and corresponding computations will be examined in sequence. A brief description of each study will be presented, including, as appropriate, the design approach, the experimental measurements, the inviscid flow computations, the boundary layer loss calculation, and the calculations from correlations for secondary flow, incidence, and tip clearance losses. Each of the five studies were examined as to the adequacy of the computational scheme to predict the experimental data. On the basis of the comparison, an evaluation or assessment of the predictive capability of the computer code will be presented. In addition, potential difficulties associated with the computational method will be identified. Specific examples will also be discussed regarding the needs for additional code verification.

The five flow examples chosen for study involved an examination of:

Kinetic energy loss coefficients in two-dimensional cascade flow (ref. 9).

Axial and tangential velocities and flow angles in an annular cascade (ref. 10, 11).

Rotor temperature and flow angle with nonuniform inlet flow (ref. 13).

Contoured endwall stator losses (ref. 12, 14).

Small axial stage stator and rotor losses (ref. 8).

The paper now proceeds to the Results section in which the five flow examples will be dicussed in sequential fashion.

RESULTS

Rectangular Cascade Flow (9)

Vane Design

The first assessment was carried out for a series of stators having turning angles from 74 to 79.6 degrees. The vanes were tested in a two-dimensional cascade in order to determine aerodynamic losses. The vane design parameters are shown in Table I. The velocity diagram for each vane was selected using a meanline turbine design calculation and a common set of inlet conditions which are representative of an advanced high bypass ratio turbofan engine. The design stator exit velocity ratio was selected so that the absolute stator exit velocity was equal to the relative rotor exit velocity. In this way, the stage kinetic energy was minimized and the losses held to a minimum. Data for a more conservative 67° vane are also included for comparison.

Surface Velocity Distributions

TSONIC, which is a finite difference inviscid stream function solution on the vane-to-vane surface (ref. 1), was used to obtain the theoretical vane surface velocity distributions. The stream sheet thickness values used in the computation were modified to account for the effects of boundary layer growth and contraction on the endwalls of the cascade tunnel and the test section. A one percent total pressure loss from vane inlet to exit was assumed.

A comparison of the experimental and theoretical velocity distributions is shown in fig. 1. Excellent agreement was obtained on the pressure side for all the vanes. The agreement on the suction surface is not as good, particularly with the higher exit angle vanes. The maximum deviation occurs with the 79.6° vane, where the theoretical value is about 10 percent higher than the data. In general, the difference between the theoretical and experimental suction surface velocity increased with vane exit angle.

Kinetic Energy Loss Coefficients

The computed velocity distributions were used as input for an integral method boundary layer code (ref. 5), BLAYER. The BLAYER code provided boundary layer parameters for an aerodynamic loss calculation (ref. 6). Laminar to turbulent transition was imposed where laminar instability was predicted by the code (momentum thickness Reynolds number of 200-300). The experimental loss values were determined in the following way. Flow angle and pressure survey data were used to calculate velocity, mass flow, and axial and tangential components of momentum as a function of the probe position. Integration of these quantities yielded overall values of the above quantities at the survey plane. The aftermix kinetic energy loss coefficient was calculated at the hypothetical aftermix station where flow conditions were assumed to be uniform. The procedure for making these calculations can be found in Appendix B of ref. 15. The experimental and theoretical losses are shown in fig. 2 at the design ideal aftermix critical velocity ratio for each vane.

Two additional computations of the losses were made. The first computation was performed in order to eliminate the effect of a variable trailing edge thickness. The experimental loss data were adjusted to a common 0.1 centimeter trailing edge thickness, using the suggestion of ref. 16, wherein ten percent blockage yields one percent loss. The theoretical losses were also recalculated on the basis of a 0.1 cm thickness. The results are shown in fig. 3a. The second additional calculation was made using the experimental velocity distributions rather than the theoretical distributions. The results are shown in fig. 3b. Both of the figures show an improvement in agreement between theoretical and experimental values.

Assessment of Analysis

The quasi three-dimensional inviscid analysis exhibited excellent prediction capability for the pressure side of all vanes, but over-predicted the suction surface velocity near the trailing edge, especially for the higher angle vanes. These theoretical velocity distributions were subsequently used to determine boundary layer parameters and loss coefficients. The difference in the theoretical and experimental loss coefficient varied from nearly zero (74.9° vane in fig. 2b) to about 25 percent (75° and 79.6° vanes in fig. 2c and 2e). The larger value of 25 percent represents an absolute loss coefficient value of about 3/4 of one percent. It is concluded, therefore, that the use of the quasi three-dimensional inviscid and boundary layer analysis for the prediction of the kinetic energy loss coefficients for high turning angle vanes is accurate to withing 3/4 of a point.

Correction of the data and analysis for trailing edge effects (fig. 3a) indicates that the computational approach described does not model the flow accurately in the base region. In addition, the improved agreement resulting from the use of the experimental velocities (fig. 3b) indicates that a source of error exists prior to the boundary layer loss calculation. Availability of a viscous analysis which treats the entire flow field simultaneously as opposed to combining an inviscid solver with a boundary layer computation, would provide a more direct computational approach for loss determination. Regardless of these considerations, it should be emphasized that the mixing and profile loss calculation for two-dimensional high turning angle vanes is accurate to within 3/4 of one point.

Annular Cascade Flow (10,11)

Cascade Experiment

The second assessment was made for the case of flow through an annular cascade having stator vanes with 67 degrees of turning as described in the previous section. A laser system was used to obtain velocity and flow angle data. The experimental stator ring assembly with the window opening on the shroud surface is shown in fig. 4. At a fixed point in the flow field, two components of velocity were measured so that magnitude and direction could be calculated. The orientation of the resultant velocity V and the flow angle α is illustrated in fig. 5.

Laser survey measurements were made at 11 axial locations within the vane passage and at an axial loca- tion 1/2 axial chord downstream of the trailing edge as shown in fig. 6. At a given axial plane, measure- ments were taken for one or more fixed radial posi- tions at 1/3-degree increments across the passage, fig. 6.

Flow Velocities and Angles

The velocity of the air flowing through the vane passage was calculated by using the inviscid two-dimensional computer programs MERIDL and TSONIC described in references 1 and 2, respectively. The MERIDL program calculates the flow on the hub-to-tip midchannel stream surface that is subsequently used in the TSONIC program to obtain a solution on a number of blade-to-blade stream surfaces from hub-to-tip. A quasi-three-dimensional solution is obtained by requiring that, for each of the TSONIC solutions, the pressure and suction-surface static pressures be equal near the vane trailing edge. This condition is obtained by slightly changing the downstream whirl distribution for the MERIDL program, repeating the TSONIC solutions, and iterating until the preceding static-pressure equality is satisfied to within some tolerance limit. This procedure (ref. 17) requires the user to make the downstream whirl distribution changes. Flow velocities and angles were also computed using the DENTON code (ref. 3, 4) which is a time marching finite volume solution of the Euler equations. At the downstream boundary the static pressure is specified at the hub and the spanwise pressure variation is calculated by the program assuming zero meridional streamline curvature (simple radial equilibrium).

Cusps are located at the vane leading and trailing edges in order to minimize discontinuities in the grid slope. The cusps carry no load and, therefore, periodicity is automatically satisfied by the DENTON program. A comparison of the theoretical and experimental flow angles and velocities are presented in fig. 7, 8, and 9 for constant axial positions of 20, 50, and 80 percent of axial chord. The results are shown for 10, 50, and 90 percent of span. The theoretical results shown were obtained from the quasi-three-dimensional inviscid TSONIC/MERIDL code and the three-dimensional DENTON code. At 20 percent axial chord, fig. 7, the TSONIC/MERIDL comparison is generally good. At the 50 percent chord position, TSONIC/MERIDL slightly overpredicts the velocity at the 50 and 90 percent span positions. At 80 percent chord, TSONIC/MERIDL underpredicts the velocity near the hub, then tends to overpredict at the midspan and vane tip locations near the pressure side, whereas the DENTON results accurately predict the velocities at the three span positions. The flow angles generally are slightly overpredicted by both codes over the entire region.

The experimental accuracy of the measurements was determined using a parameter estimation technique and comparisons were made with the computed results. The velocity magnitudes using TSONIC/MERIDL and DENTON at 20 percent axial chord were found to fall outside the measurement uncertainty band by 1.0 and 0.4 percent, whereas the flow angles fell inside the band. The uncertainty band for the measurements was approximately 1.0 percent for the seed particle measurement and less than 2.0 percent for seed particle lag. The corresponding flow angle uncertainties were 1.4° and less than 1°. At 50 percent axial chord, the corresponding values were 2.0 and 0.7 percent for the velocities, and 0.1° for the flow angles. At 80 percent axial chord, the percentages for the velocities were 2.0 and 0.4 and for the flow angles were 0.1° and 0.2°.

Assessment

Inspection of the overall results shows that both of the inviscid codes accurately predict two components (axial and tangential) of velocity and the corresponding flow angle through a 67° annular stator cascade. Velocity magnitudes are predicted to within 2 percent and flow angles to within 0.2 degree of the uncertainty band. The largest differences occur near the endwall and toward the vane exit, where viscous and secondary flow effects are the largest. A more critical assessment of the computer codes will be made when the radial component of the velocity is measured. Also, the inviscid codes will be put to a more stringent test when applied to the prediction of the flow field in higher turning angle stators (i.e., 75 to 80°), where stronger secondary flows will be generated. Some evidence that the DENTON code will not model regions of strong secondary flows is presented in refs. 18 and 19. The results of refs. 18 and 19 are not surprising in view of the fact that the secondary flows due to viscous effects (i.e., endwall boundary layer and vane leading edge interaction) is not accounted for in the inviscid codes. However, until such time as the above mentioned assessments are performed, it is concluded that the inviscid codes described accurately predict the two components of velocity and the flow angle in a stator.

Non-Uniform Turbine Inlet Temperature Flow (13)

Turbine Design

The third assessment was made for a 20-inch rotor diameter low aspect ratio turbine stage with nonuniform radial temperature distribution at the stator entrance. Fig. 10 shows the turbine inlet temperature distributions with and without the Combustor Exit Radial Temperature Simulator (CERTS). The corresponding inlet total pressure distributions are shown in fig. 11. The stators vanes were designed for 75 degrees of turning and were similar to that described in section 1 entitled "Rectangular Cascade Flow." Total temperatures, flow angles, and pressures were measured at inlet and exit planes.

Secondary Flow and Temperatures

The inviscid rotational code developed by Denton was also used to obtain the analytical results. The code is a three-dimensional time-marching solver of the unsteady Euler equations in finite-volume form for fixed or rotating turbomachinery blade rows (refs. 3, 4). Good resolution of the blade profiles was obtained by using nonuniform grid generation. The grid used for the stator vane channel was 19 (pitch) x 19 (span) x 58 (axial). The corresponding grid dimensions for the rotor blade channel were 10 x 19 x 68. Computational time was reduced by using a two-level multigrid technique. The code was run for

the stator with the measured inlet temperature and pressure profiles from the experiment, both with and without CERTS, as are shown in fig. 10 and 11. The stator exit velocity was matched to the experimental data by specifying appropriate static pressures at the stator exit hub and tip. The computed results at the stator exit were then circumferentially averaged using mass flow weighting and used as inlet conditions for the rotor. The rotor exit velocity was matched to the experimental data by specifying appropriate static pressures at the rotor exit hub and tip. The computed results at the rotor exit were also circumferentially averaged to allow comparison with the experimental survey results obtained from probes in the stationary frame.

The secondary flow pattern computed with the Denton code is shown in fig. 12 for the midchord position of the rotor. The flow movement, from suction to pressure surface, causes a redistribution of the inlet temperature profile. The hot flow at the midspan position shifts toward the endwalls at the pressure surface and the cooler endwall fluid moves toward the midspan region at the suction surface.

Figure 13 compares the analytical and experimental rotor exit temperature profiles with and without CERTS. The results indicate that the CERTS temperature profile is mixed out at the exit survey plane, although the analytical profile indicates a lack of mixing (see fig. 13). The slight temperature drop in the experimental data at the tip endwall is attributed to heat transfer through the casing. The computed profile without the simulator, fig. 13, shows close agreement with the data with the exception at the tip endwall.

Rotor Flow Angles

The rotor exit angles are shown in fig. 14. For the test with the simulator, close agreement is observed at the hub, while large differences are seen at midspan and tip. The difference at the tip is believed to be due to increased clearance due to the use of coolant air with the simulator (0.5 percent clearance without CERTS versus 1.1 percent with CERTS). The flow angles without the simulator, fig. 14, show close agreement at the tip. However, the midspan flow shows a substantial difference between theory and experiment. A significant amount of underturning occurs at the midspan of the rotor

Assessment

In contrast to the good agreement shown in the previous section between computed and measured flow angles for the annular cascade, the predicted flow angle from the rotor is in severe disagreement with the measured data. The experimental rotor exit flow angles had 11 to 14 degrees less turning than predicted by the DENTON code. The occurrence of this severe underturning is believed to be partly due to the low aspect ratio of the blades which give rise to strong secondary flow over a large portion of the span. As noted previously, it may not be possible to compute the strong secondary flow fields with the DENTON code. This is due to the fact that only the rotational portion of the secondary flow is computed whereas the viscous contributions (i.e., vortex formation) is not accounted for in an Euler code. An additional factor contributing to the discrepancy between the experimental and measured flow angles may be the interaction between the stator and rotor secondary flow fields which is not accounted for in the analysis. The computed results at the stator exit were circumferentially mass averaged and then used as inlet conditions for the rotor. The rotor inlet flow field used for the DENTON computations, therefore, does not correspond to the physical flow field.

The discrepancy noted in the flow angles of the present flow example suggests that the inviscid rotational code is unable to predict the strong secondary flows present in a rotor passage and that a three-dimensional viscous code may be required in order to accurately predict rotor flow fields.

Contoured Endwall Stator Flow (12, 14, 17)

Endwall Design

The fourth assessment was carried out on the effect of stator endwall contouring on flow losses in a small annular cascade. Two different contoured endwall stator geometries were designed and tested for comparison with a cylindrical geometry. The same vane profile shape (ref. 12) was used for all three configurations. The three geometries are shown in fig. 15; a cylindrical, an S-shape, and a conical geometry. The vane surface velocities for the three stators are shown in fig. 16. These were obtained by using the MERIDL/TSONIC codes (refs. 1, 2). For those cases where supersonic flow occurred, Wood's modification was used (ref. 20). At the hub and mean positions, the surface velocities were slightly lower for the two contoured stators, a result of the increased inlet passage height. At the tip, when configuration A turns the flow radially inward, the surface velocities decreased, followed by a large overshoot in the suction surface velocity. The computed pressure distributions along the suction surfaces of the three stator configurations are shown in fig. 17. It may be seen in fig. 17a that the pressure gradient from the leading edge to about 70 percent chord will drive the flow from hub to tip. Near the stator exit, the pressure becomes lower near the hub, and the low momentum fluid along the tip wall would migrate to the hub wall. Contoured stator A, fig. 17b, has a pressure distribution which would prevent migration of low momentum fluid from the hub beyond midspan. At about 80 percent of the axial chord, a low pressure region occurs near the tip, trapping low momentum fluid in that location. Stator contour B, fig. 17c, has less severe pressure gradients and hence there is not a strong driving force to move low-momentum fluid to either the hub or tip regions. From these data it appears that a significant effect of endwall contouring is to reduce the radial migration of low-momentum fluid.

Kinetic Energy Loss Coefficient

The stator kinetic energy loss coefficient was calculated from flow angle and total pressure surveys. The calculation was based on the determination of complete mixing at a hypothetical downstream station as described in the section entitled "Rectan-

gular Cascade Flow." The losses, computed in this fashion, are shown in fig. 18 for the three geometries at the design stator pressure ratio of 1.8 and also for 1.35. The data show that the cylindrical stator had lower losses near the tip and higher losses near the hub than the two contoured stator configurations. It appears that the effect of contouring is to change the radial distribution of loss. For the two contoured stator configurations, the loss region remained near the tip instead of migrating radially inward toward the hub as was the case for the cylindrical stator. These experimental observations are in agreement with the conclusions drawn from the computed suction surface pressure distributions shown in fig. 17 and dicussed in the previous section. The overall kinetic energy loss coefficients were approximately 0.5 percent lower for the two contoured geometries than was the cylindrical.

MERIDL/TSONIC and BLAYER were used to calculate the aftermix kinetic energy loss coefficients for both the vane profile and the endwalls. The profile loss included the friction loss along the suction and pressure surfaces, and the mixing loss. The endwall loss was the total friction loss along the hub and tip endwalls up to the axial measuring station.

The experimental values of typical kinetic energy loss coefficients at design equivalent speed and stage pressure ratio are compared with the computed values in the upper portion of Table II. The computed results include the secondary losses as well as an incidence loss. The correlation of Morris and Hoare (ref. 7) was used for the secondary loss calculation with one modification, i.e., only the inlet displacement thickness term was used since the BLAYER calculation already accounted for the downstream boundary layer losses. The comparison in Table II shows that the calculated losses were 0.005 etc. and 0.004 lower for stator contours A and B than the cylindrical contour. In addition, the measured loss coefficients were 0.003 lower for stators A and B than the cylindrical stator. The computed loss coefficients were in error by only 1.8, 5.8, and 3.8 percent, respectively, relative to the measurements, for the cylindrical, contour A and contour B stators. The difference in stator pressure ratio for the three configurations was due to variations in the stator-rotor throat area ratios. This effect is addressed in the following section on Small Axial Stage Flow.

Assessment

The aftermixed kinetic energy loss coefficient calculated from MERIDL/TSONIC with BLAYER and the secondary flow losses using the correlation of Morris and Hoare yielded values which agreed closely with the overall measured stator loss. Both the analysis and experiment showed that the reduction in loss with contouring was small for the lightly loaded configurations used in this study. A more meaningful case would involve a highly loaded stator configuration in which the radial and cross channel gradients, and hence, the secondary flows, would be greater. Most of the loss reduction with the contoured stators was attributed to a reduction in boundary layer growth along the vanes and endwall surfaces.

On the basis of the comparisons between the computed results and the experimental data, the combined inviscid-correlative approach or (coupled analysis) appears to have the potential of accurately predicting stator performance. The difficulty with this analytical approach is that the accuracy of the individual loss calculations is not amenable to verification. Profile and mixing losses, endwall friction losses, secondary flow losses, and incidence losses for the stator rings cannot be experimentally determined on an individual basis. The only measure of success is the comparison of overall experimental loss with the sum of the individual calculated losses. In addition, since the reduction in the loss coefficient appears to be associated with a redistribution of losses across the passages, one would expect that a reliable computational approach must be capable of treating the secondary flows that occur in a turbine passage. The analytical approach requires a formulation which treats the secondary flow generated by vane leading edges as well as by passage turning.

In spite of the considerations discussed above, it is noted that the computed stator losses are in excellent agreement with the experimental data. Until further assessment is carried out, it is concluded that the three-dimensional inviscid approach coupled with an integral boundary layer and loss correlations provides a highly accurate technique for computing losses in a stator row.

Small Axial Stage Flow (8)

Geometric Configuration

The three stator configurations described in the preceeding section, "Contoured Endwall Stator," were tested with a common rotor to determine the effect of contouring on overall stage performance. It is currently believed that contouring reduces the radial and cross-channel pressure gradients and reduces boundary layer growth, thus inhibiting the movement of low momentum fluid and reducing loss. Further testing was carried out using a small (12.8- centimeter diameter) axial flow turbine.

Loss and Efficiency Calculation

The losses for the three configurations were calculated using MERIDL/TSONIC, BLAYER, and Morris and Hoare's correlation as described previously and in ref. 8. The analysis used the experimental values of turbine inlet temperature, pressure, mass flow, wall displacement and stator pressure ratio. Table II shows the breakdown of the individual losses calculated for both the stator and the rotor. As seen in the previous section (Contoured Endwall Stator Flow), the calculated total stator kinetic energy loss coefficents were within 0.003 of the measured values. Inspection of the rotor losses shows that there is a substantial reduction in the calculated total rotor kinetic energy loss coefficient for the two contoured stators relative to the cylindrical geometry. When the rotor loss coefficient is converted into stage efficiency loss (ref. 8), the values are nearly constant for all three stator configurations. (i.e., 0.104, 0.101, 0.101). This effect is due to the fact that the two contoured

stages have higher rotor pressure ratios. (Loss computations were also made for stator configurations A and B with rotated vanes so that the same stator and rotor pressure ratios were achieved as with the cylindrical geometry. The results caused only minor changes to the values in Table II and had no effect on the conclusions.) Addition of the computed stator and rotor losses yields overall stage efficiencies of 0.856, 0.865, and 0.863 for the cylindrical, stator A and stator B configurations, respectively. The corresponding measured values of the stage efficiencies were 0.845, 0.851, and 0.853.

Assessment

Using the detailed data presented in Table II it is possible to compare the calculated efficiency losses ($\Delta n'$) with those measured for the three geometric configurations. This was done by converting the measured stator kinetic energy loss coefficient to a stage efficiency loss using the expression in ref. 8. For the case of the cylindrical contour, the measured values $\bar{e}$ of 0.055 converts to a $\Delta n'$ value of 0.036. The computed value of the efficiency loss (0.035) is within 2.8 percent of the measured value. For contour A, the difference between calculated and measured $\Delta n'$ is 6.9 percent; and for stator B, the value is zero. As observed earlier, the ability to compute stator losses with a combined inviscid-boundary layer-correlative approach for these geometries appears to be excellent. Since the rotor efficiency loss cannot be measured separately, the efficiency losses for the stator and exhaust duct were summed and deducted from the measured stage efficiency loss. That is: $\Delta n'_{rotor} = \Delta n'_{stage} - (\Delta n'_{stator} + \Delta n'_{exhaust\ duct})$. Hence, for the cylindrical geometry, the sum of the measured stator efficiency loss (0.036) and the duct efficiency loss (0.005) were subtracted from the measured stage efficiency loss (0.155) to yield a "measured" rotor efficiency loss (0.114). The computed value of the rotor efficiency loss for the cylindrical configuration (0.104) shows a difference of 8.8 percent relative to the measured value. Likewise, the difference between the computed and measured rotor efficiency loss for contour A was 10.6 percent and for contour B was 9 percent. These results for the stator and rotor indicate that improvements in the computation of turbine efficiency require greater accuracy in the rotor passage. In view of the spanwise redistribution of low-momentum fluid and the associated transverse flows that occur as the flow leaves the contoured stator passage and enters the rotor passage, a three-dimensional viscous analysis may be required to improve the accuracy of the rotor flow field calculation.

It is noted that the results discussed above were obtained with high solidity stator blading, accompanied by light loading and well accelerated flow. The ability of the analysis to predict the losses in lower solidity blading with higher loading is not yet assessed.

CONCLUSIONS

Comparisons between measured and computed aerodynamic parameters have been examined in an effort to evaluate current computational capabilities. Specifically, the ability of the inviscid TSONIC code, an integral boundary layer code (BLAYER) and a mixing loss model by Stewart to compute the kinetic energy loss coefficients for a series of two-dimensional high turning angle vanes was examined. It was concluded that the computational procedure was accurate to within 3/4 of one point in loss coefficient. It was further concluded that improvements in the computation could result from improved flow modeling in the trailing edge region. Improvement is also desirable in the computation of the suction surface velocity distribution.

The second evaluation was carried out for annular cascade flow for which experimental laser measurements of two velocity components and flow angle were available. These data were compared with the results of the quasi-three-dimensional inviscid TSONIC/MERIDL code and the three-dimensional inviscid DENTON code. It was concluded that both of these codes accurately predicted the axial and tangential velocity components and the corresponding flow angle through a 67° turning vane. Additional evaluation of the two codes needs to be carried out for the radial velocity component and for higher turning angle vanes with significantly larger secondary flows.

A third assessment was performed of the ability of the DENTON code to predict the temperature and flow angles downstream of a single stage turbine operated with and without a radial variation in entrance temperature. The three-dimensional inviscid DENTON code gave reasonable agreement with the rotor exit temperature profiles but was in poor agreement with the rotor exit flow angle distributions. The computation does not predict the significant underturning at the midspan rotor position that is measured experimentally. It was concluded that the strong secondary flows present in the low aspect blades may not be sufficiently well modeled in the code. In addition, the inviscid rotational approach is unable to account for realistic rotor inlet conditions and stator-rotor interaction. Development of a three-dimensional viscous analysis for the rotor flow fields appears necessary.

A fourth evaluation was performed regarding the ability of TSONIC/MERIDL, BLAYER and a series of loss correlations to predict the losses in contoured stator rings. Comparison of the calculated stator kinetic energy loss coefficients with the measured values show excellent agreement. Further assessment of the computational approach is required for more highly loaded stator configurations than those available for comparison. A difficulty with the present approach is that individual loss comparisons can not be performed for annular configurations. This situation creates a problem in attempting to evaluate the benefits of contouring versus leaning versus bowing versus sweeping. Significant deviations from two-dimensionality will give rise to cross-channel variations and influence the ability to predict secondary flow phenomena accurately.

The final assessment was on the application of the TSONIC/MERIDL, BLAYER, and loss correlations to a small axial stage with contoured endwalls. This comparison made use of the results described above for the contoured stators by the addition of a common rotor. The computed rotor losses were compared to the experimental measurements. It was concluded that additional improvements are needed for the rotor flow

field computations.

In summary, the ability to compute losses and flow fields within two-dimensional and annular cascade passages has evolved to a high degree of accuracy, with some exception. In contrast, the ability to predict the flow field and the losses occurring in the rotor is much less accurate. In view of the highly complex nature of the flow field that may occur in a turbine passage, and a strong desire to exploit novel stator and rotor geometries, development of an accurate three-dimensional viscous code is necessary.

SYMBOLS:

b	trailing edge blockage factor, $t/s \cos \alpha$
c_x	vane axial chord, cm
e	kinetic energy loss coefficient, $1 - (V/V_{id})^2$
p, P	absolute pressure, N/cm^2
R	radial position
R_x	rotor reaction, ΔP rotor/ΔP stage
s	vane pitch, cm
t	trailing edge thickness, cm
T	temperature, K
V,U	velocity, m/sec
V_1, V_2	velocity components (see fig. 5)
w	mass flow rate per unit vane span, kg/sec-cm
Z	axial position
α	flow angle or absolute swirl angle, degrees
θ	angular position (fig. 6)
η	efficiency
σ_x	axial solidity factor, c_x/s
Ψ	Zweifel loading factor
ϕ	flow angle (see fig. 5)

SUBSCRIPTS:

cr	critical condition
id	ideal process
m	mean
s	vane surface
1	stator inlet
2	stator aftermix station
2.5	station 0.52 cm downstream of vane trailing edge
3M	aftermix station

SUPERSCRIPTS:

'	total state condition
-	mean

REFERENCES

1. Katsanis, T., "FORTRAN Program for Calculating Transonic Velocities on a Blade-to-Blade Stream Surface of a Turbomachine," NASA TN D-5427, 1969.

2. Katsanis, T., and McNally, W. D., "Revised FORTRAN Program for Calculating Velocities and Streamlines on the Hub-Shroud Midchannel Stream Surface of an Axial-, Radial-, or Mixed-Flow Turbomachine or Annular Duct," I--User's Manual. NASA TN D-8430, 1977.

3. Denton, J.D., and Singh, U.K., "Time Marching Methods for Turbomachinery Flow Calculation. Part I--Basic Principles and 2D Applications and II Three Dimensional Flows," Application of Numerical Methods to Flow Calculations in Turbomachine, VKI Lecture Series 1979-7, 1979.

4. Denton, J.D., "An Improved Time Marching Method for Turbomachinery Flow Calculation," ASME Paper 82-GS-239, Apr. 1982.

5. McNally, W. D., "FORTRAN Program for Calculating Compressible Laminar and Turbulent Boundary Layers in Arbitrary Pressure Gradients," NASA TN D-5681, 1970.

6. Stewart, W. L., "Analysis of Two-Dimensional Compressible Flow Loss Characteristics Downstream of Turbomachine Blade Rows in Terms of Boundary Layer Characteristics," NASA TN-3515, 1955.

7. Morris, A.W.H., and Hoare, R.G., "Secondary Loss Measurements in a Cascade of Turbine Blades with Meridional Wall Profiling," ASME Paper No. 75-WA/GT-13, Nov. 1975.

8. Haas, J. E., and Boyle, R. J., "Analytical and Experimental Investigation of Stator Endwall Contouring in a Small Axial-Flow Turbine, Part II: Stage Performance," Proposed NASA technical paper.

9. Schwab, J. R., "Aerodynamic Performance of High Turning Core Turbine Vanes in a Two-Dimensional Cascade," NASA TM-82894, 1982.

10. Goldman, L. J., and Seasholtz, R. G., "Laser Anemometer Measurements in an Annular Cascade of Core Turbine Vanes and Comparison with Theory," NASA TP-2018, 1982.

11. Goldman, L. J., and Seaholtz, R. G., "Comparison of Laser Anemometer Measurements and Theory in an Annular Turbine Cascade with Experimental Accuracy Determined by Parameter Estimation," Engineering Applications of Laser Velocimetry, H. W. Coleman and P. A. Pfund, eds., AMSE, 1982.

12. Haas, J. E., "Analytical and Experimental Investigation of Stator Endwall Contouring in a Small Axial Flow Turbine. I: Stator Performance," NASA TP-2023, 1982.

13. Schwab, J. R., Stabe, R. G., and Whitney, W. J., "Analytical and Experimental Study of Flow Through an Axial Turbine Stage With a Nonuniform Inlet Radial Temperature Profile," AIAA Paper 83-1175, June 1983.

14. Boyle, R. J., and Haas, J. E., "Comparison of Experimental and Analytic Performance for Contoured Endwall Stators," NASA TM-82877, AVRADCOM TR 82-C-12, June 1982.

15. Goldman, L. J., and McLallin, K. L., "Cold-Air Annular-Cascade Investigation of Aerodynamic Performance of Cooled Turbine Vanes. I: Facility Description and Base (Solid) Vane Performance," NASA TM X-3006, 1974.

16. Prust, H. W. Jr., Moffitt, T. P., and Bider, B., "Effect of Variable Stator Area on Performance of a Single-Stage Turbine Suitable for Air Cooling. V: Stator Detailed Losses with 70-Percent Design Area," NASA TM X-1696, 1968.

17. Boyle, R. J., Rohlik, H. E., and Goldman, L. J., "Analytic Investigation of Effect of Endwall Contouring on Stator Performance," NASA TP-1943, 1981.

18. Schwab, J. R., and Povinelli, L. A., "Comparison on Secondary Flows Predicted by a Viscous Code and an Inviscid Code with Experimental Data for a Turning Duct," ASME Fluids Engineering Conference, Feb. 1984.

19. Dawes, W.N.; and Richards, P.H , "A Comparison of Experimental and Numerical Results Obtained for the Secondary Flow in a Large Turbine Cascade," Journal of Physics Design: Applied Physics, Vol. 16, No. 4, Apr. 14,1983, pp. 539-551.

20. Wood, J.R., "Improved Method for Calculating Transonic Velocities on Blade-to-Blade Stream Surfaces of a Turbomachine," NASA TP-1772, 1981.

TABLE I--VANL DESIGN PARAMETERS

Aftermix flow angle, α, degrees	Aftermix velocity ratio, $(V/V_{cr})_2$	Trailing-edge blockage factor, b	Axial solidity factor, σ_x	Zwiefel loading factor, Ψ
67.0	0.778	0.111	0.929	0.774
74.9	.843	.079	.716	.701
75.0	.833	.127	.630	.792
77.5	.810	.124	.537	.790
79.6	.795	.076	.439	.813

TABLE II--CALCULATED AND MEASURED STATOR AND ROTOR LOSSES

	Cylindrical Stator	Contoured Stator A	Contoured Stator B
CALCULATED STATOR LOSSES ($\bar{e}$):			
Profile and mixing	0.029	0.027	0.026
Endwall friction	.018	.017	.016
Secondary	.006	.005	.008
Incidence	.001	.000	.000
Total	0.054	0.049	0.050
Δn'stage	.035	.027	.031
Total-to-Static pressure ratio across stator	2.01	1.82	1.91
MEASURED STATOR $\bar{e}$	.055	.052	.052
CALCULATED ROTOR LOSSES ($\bar{e}$):			
Profile and mixing	.034	.031	.031
Hub endwall friction	.007	.006	.007
Secondary	.022	.017	.020
Incidence	.024	.097	.014
Tip Clearance	.086	.013	.085
Disk windage	.002	.002	.002
Total	.176	.146	.159
Δn'stage	.104	.101	.101
Total-to-Static pressure ratio across rotor	1.87	2.06	1.96
EXHAUST DUCT LOSS, Δn'stage	.005	.007	.005
OVERALL STAGE EFFICIENCY	.856	.865	.863
R_x	.271	.355	.315
stage pressure ratio	2.77	2.77	2.77
MEASURED STAGE EFFICIENCY	.845	.851	.853

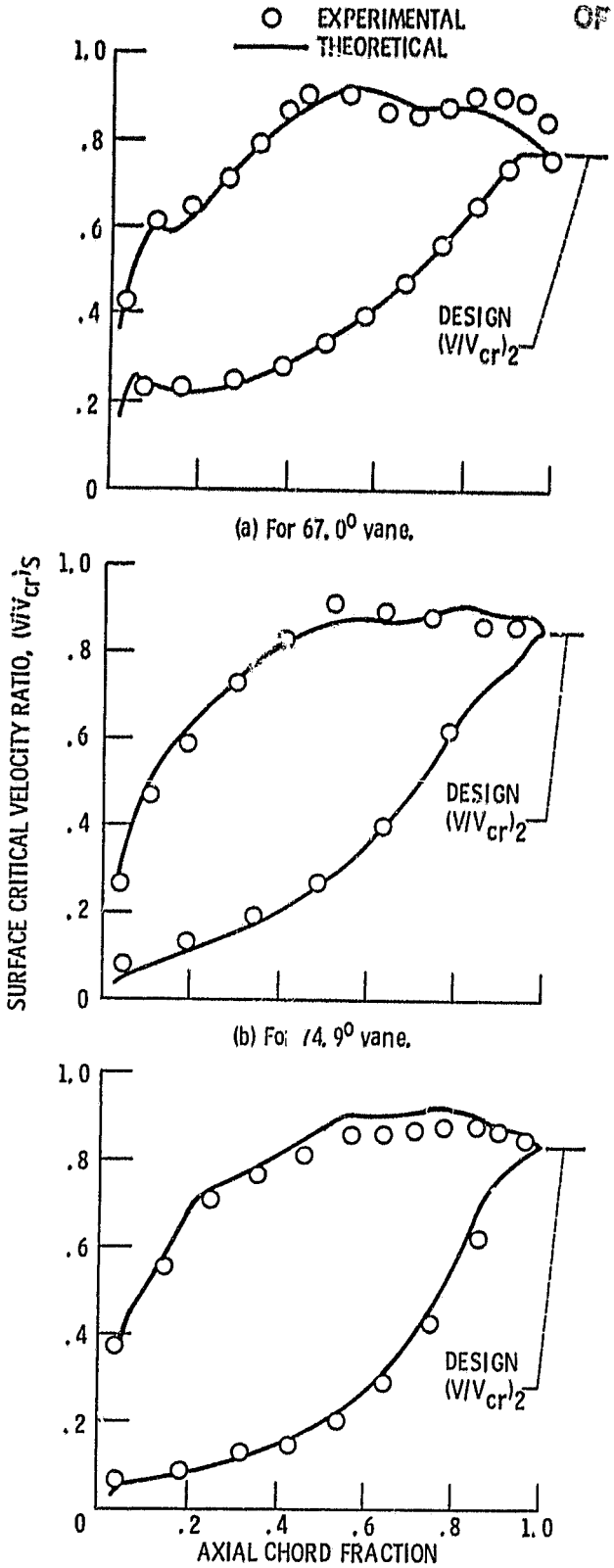

(a) For 67.0° vane.

(b) For 74.9° vane.

(c) For 75.0° vane.

Figure 1. - Surface velocity distribution.

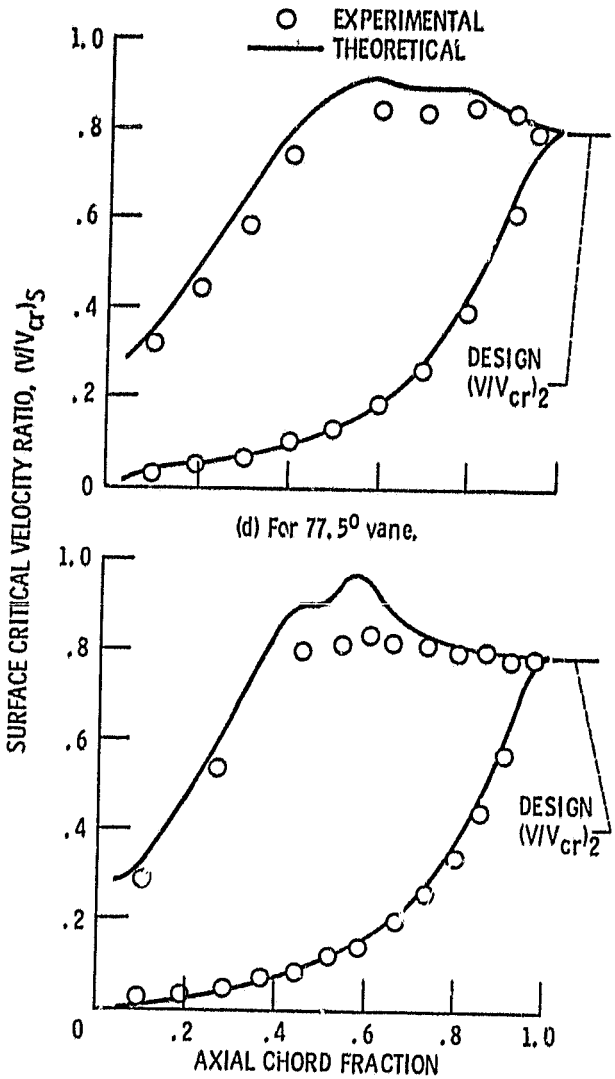

(d) For 77.5° vane.

(e) For 79.6° vane.

Figure 1. - Concluded.

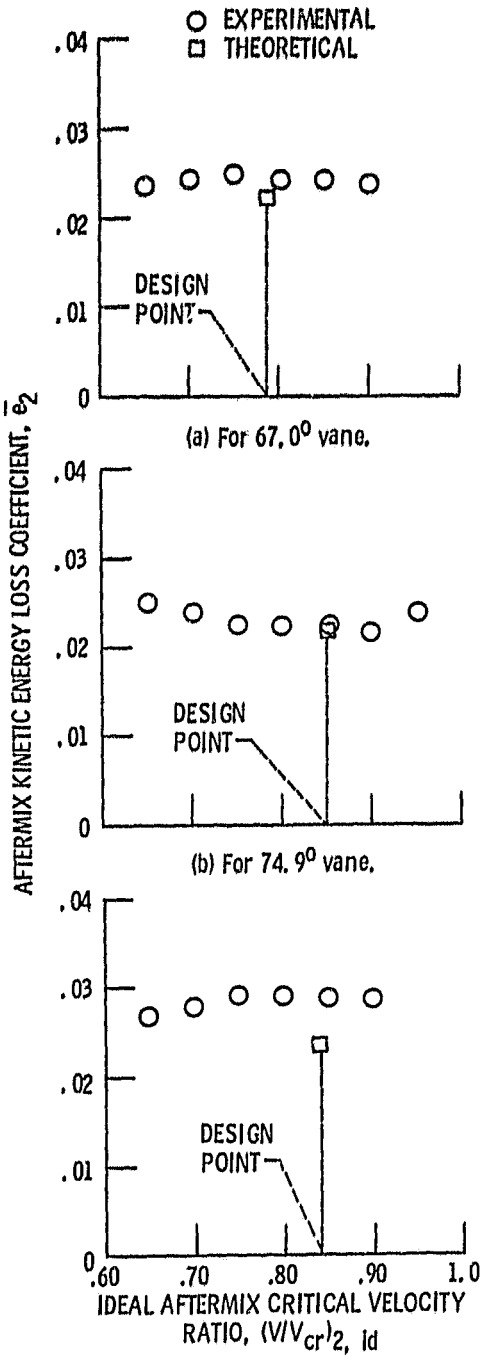

(a) For 67.0° vane.

(b) For 74.9° vane.

(c) For 75.0° vane.

Figure 2. - Kinetic energy losses.

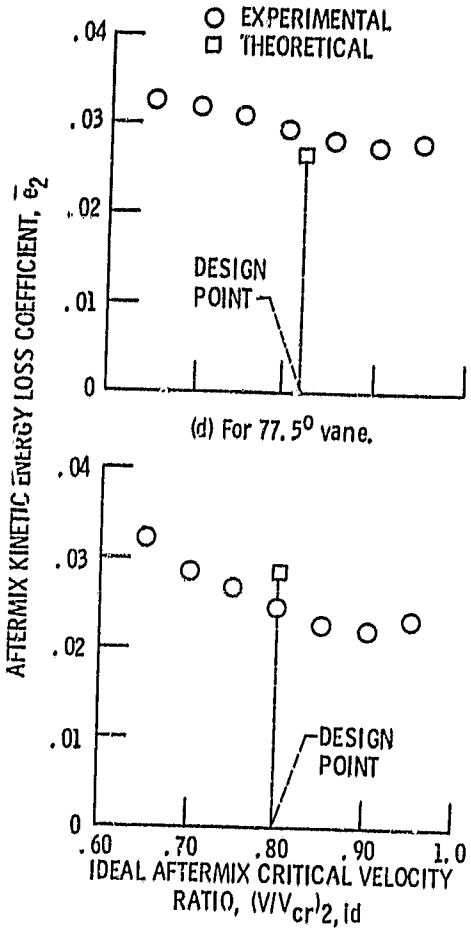

(d) For 77.5° vane.

(e) For 79.6° vane.

Figure 2. - Concluded.

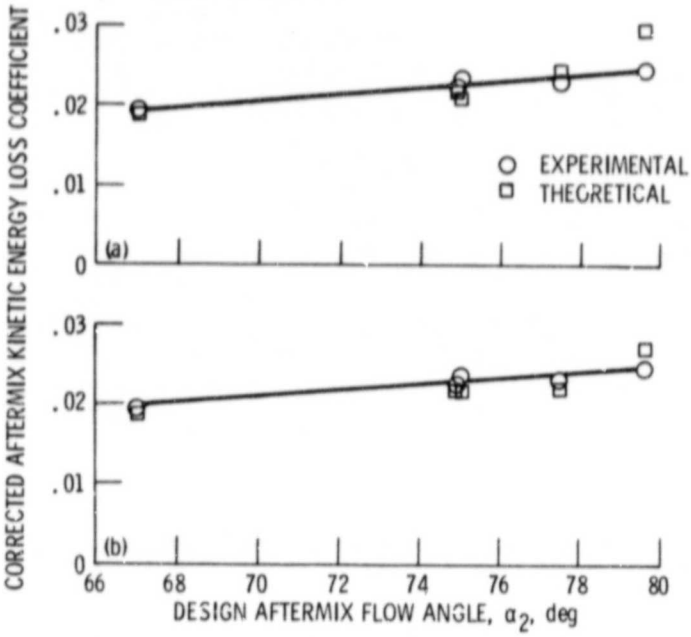

Figure 3. - Comparison of experimental losses corrected to 0.100 cm trailing edge thickness with theoretical losses calculated using 0.100 cm trailing edge thickness and experimental surface velocity distributions.

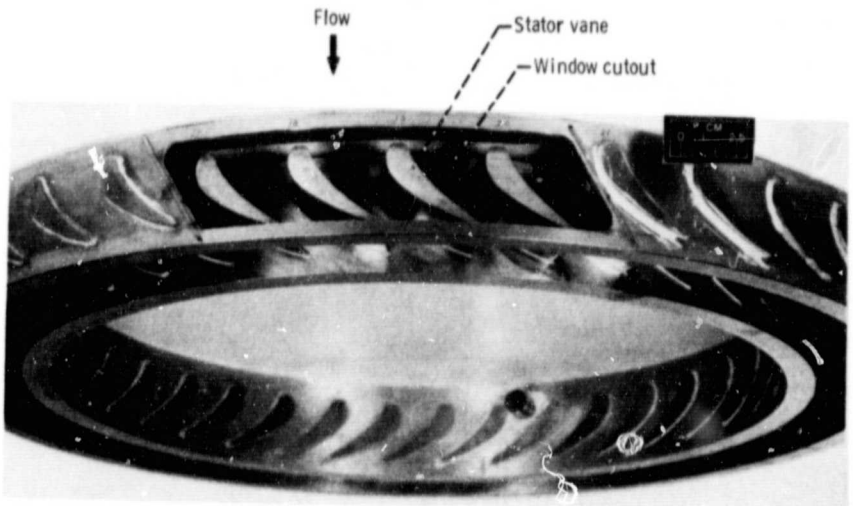

Figure 4. - Stator vane ring showing cutout for laser windows.

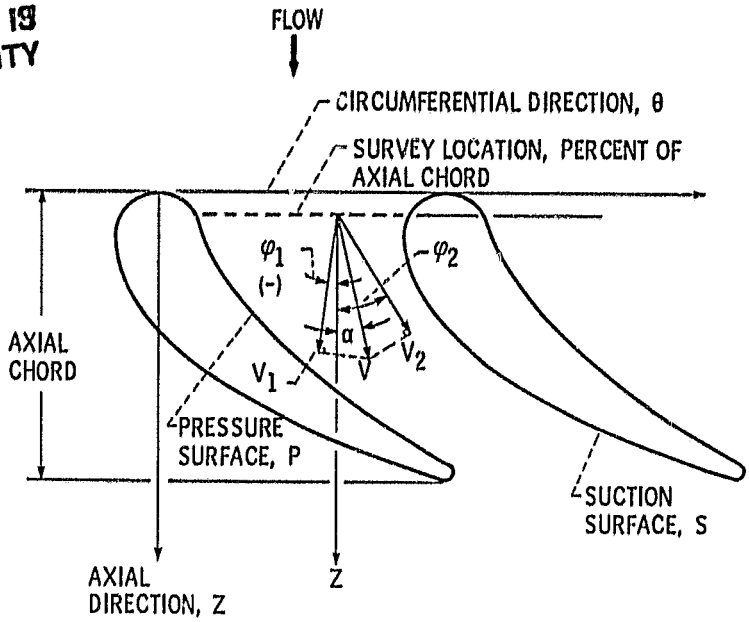

Figure 5. - Nomenclature and orientation of velocity component measurements for laser anemometer surveys.

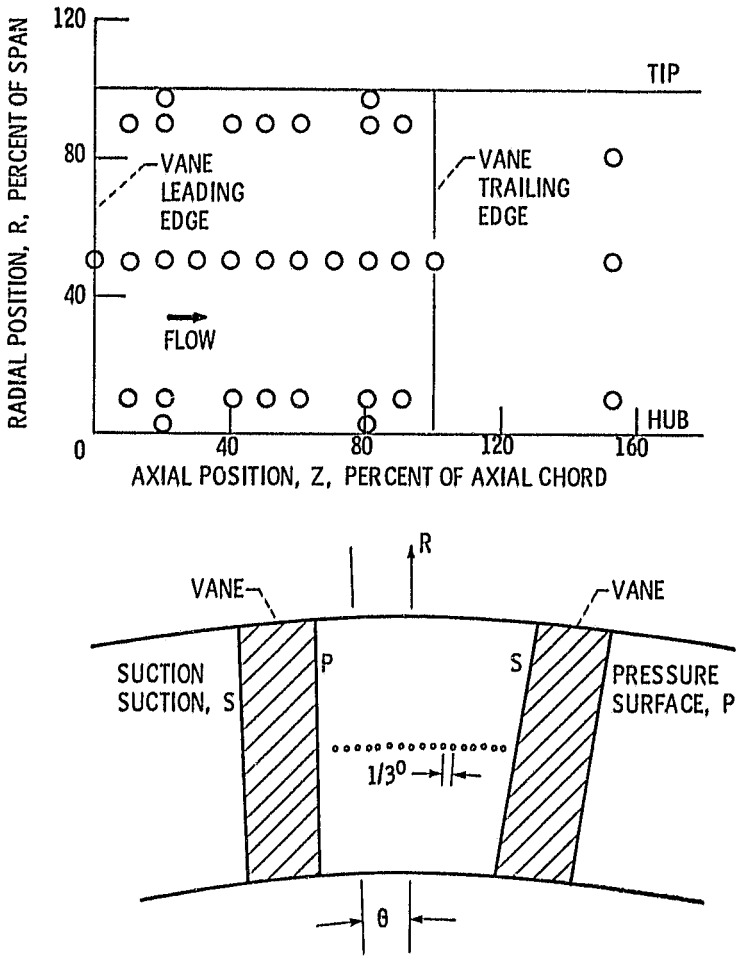

Figure 6. - Laser survey measurement locations.

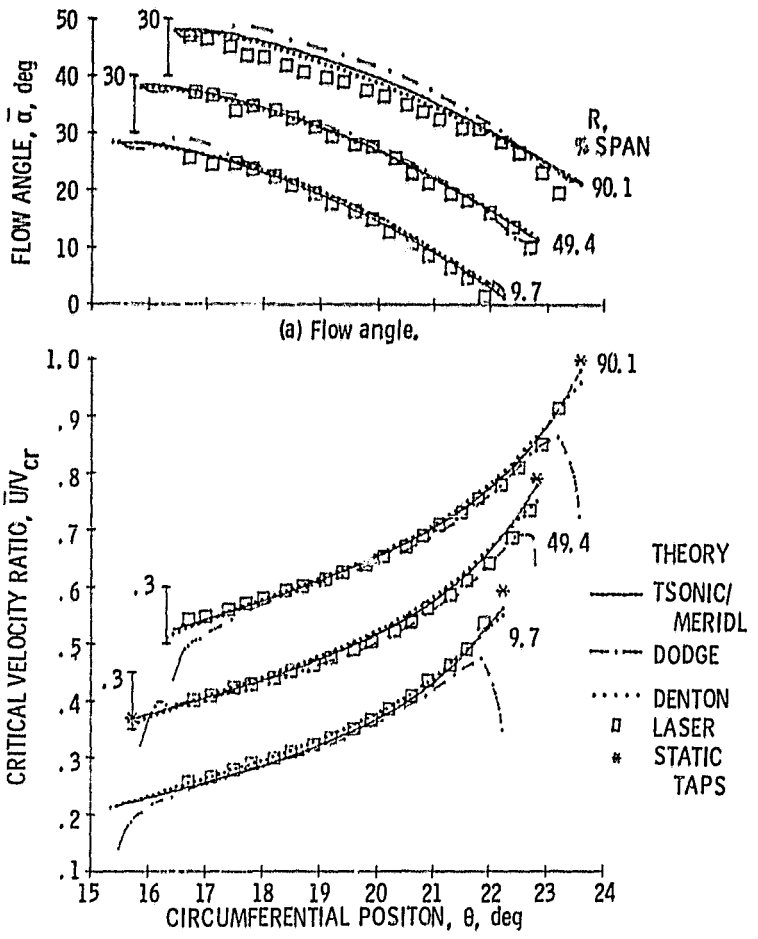

Figure 7. - Comparison of laser measurements with theory at 20.0 percent axial chord.

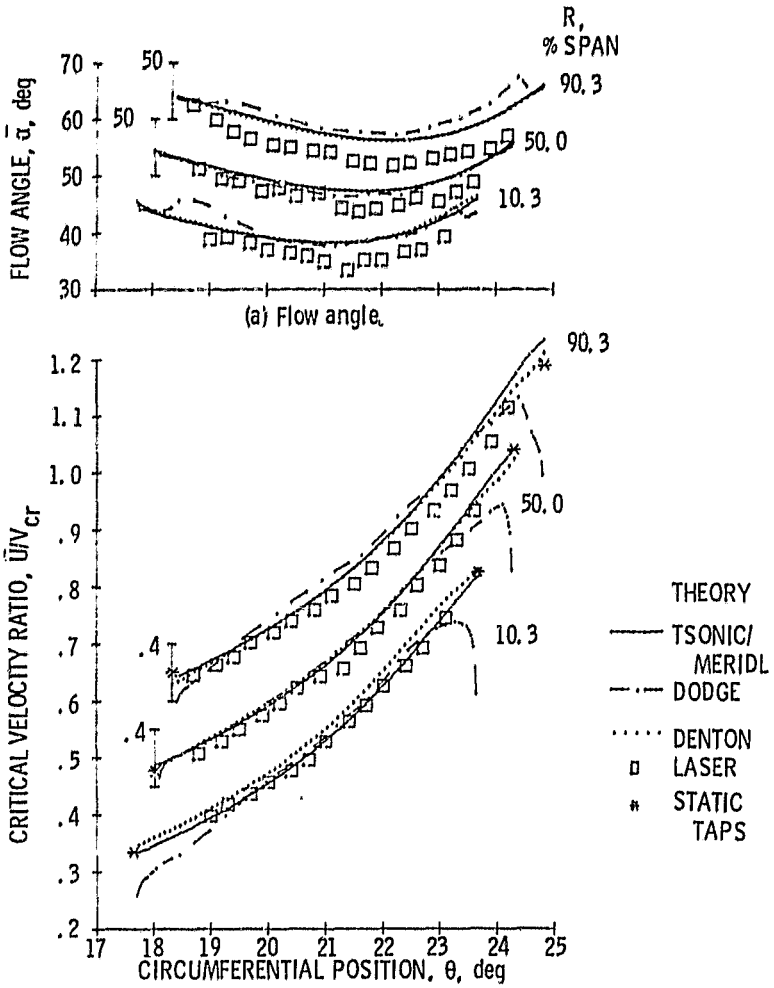

(b) Critical velocity ratio.

Figure 8. - Comparison of laser measurements with theory at 50.0 percent axial chord.

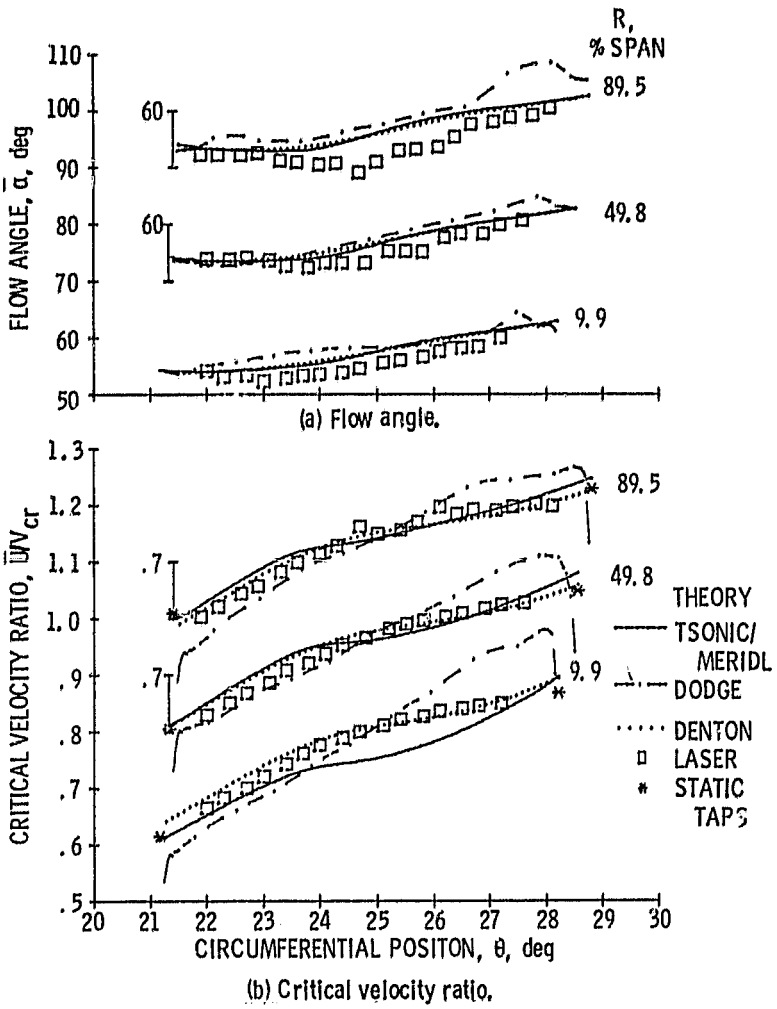

Figure 9. - Comparison of laser measurements with theory at 80.0 percent axial chord.

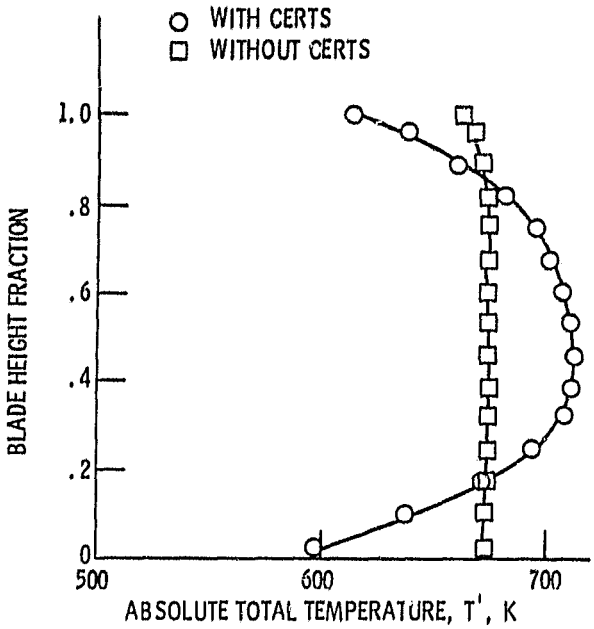

Figure 10. - Stator inlet temperature profiles.

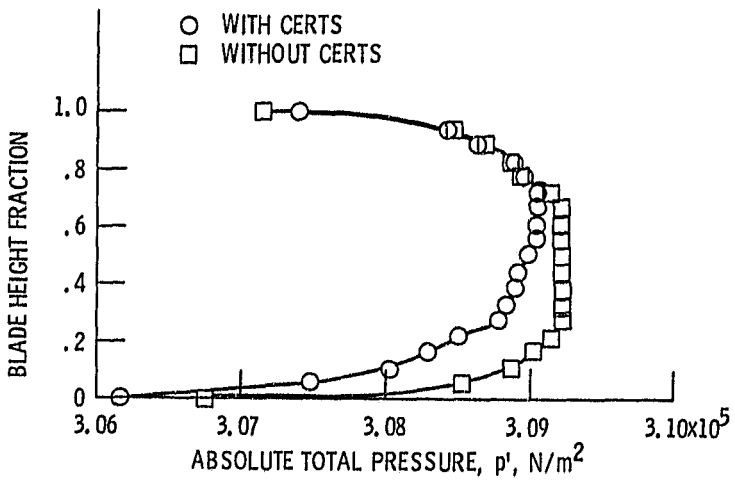

Figure 11. - Stator inlet pressure profiles.

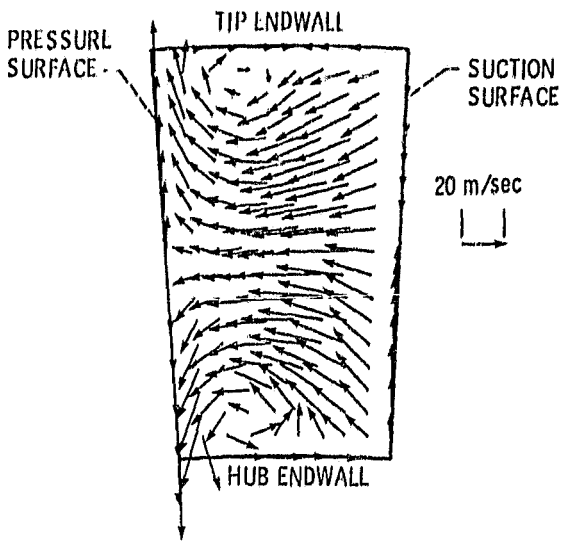

Figure 12. - Computed relative secondary flow vectors at rotor blade mid-chord.

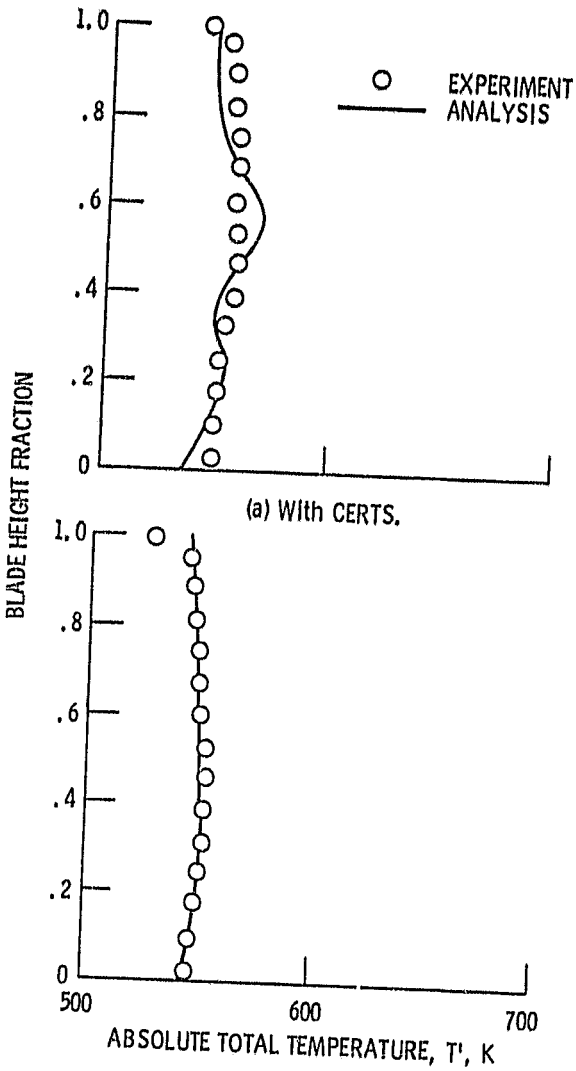

Figure 13. - Rotor exit temperature profiles.

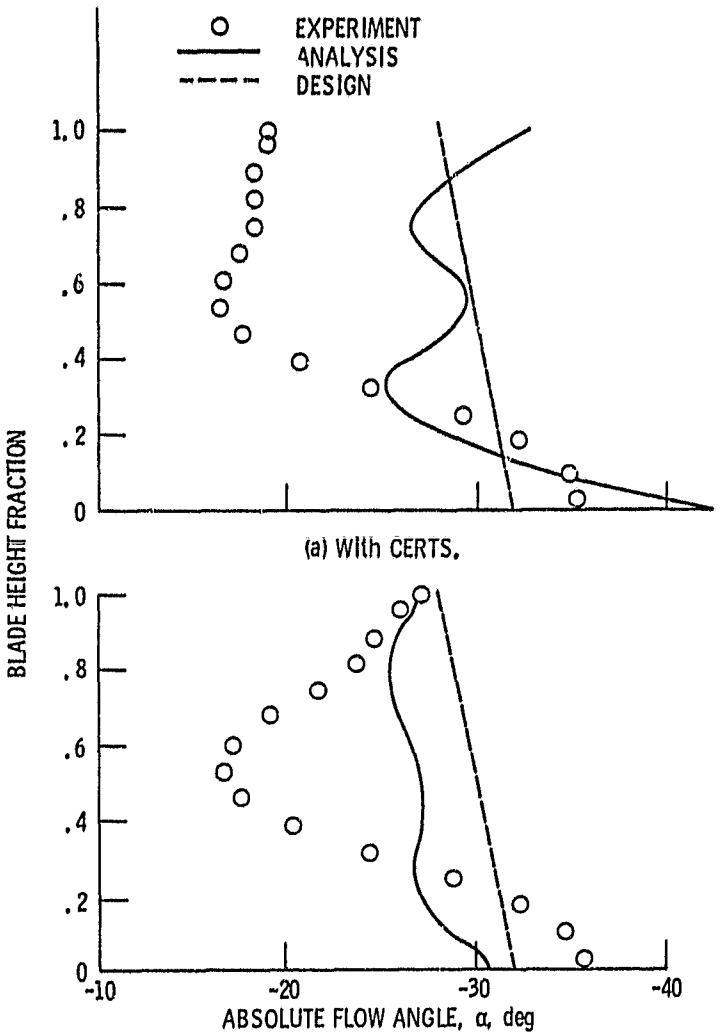

(a) With CERTS.

(b) Without CERTS.

Figure 14. - Rotor exit flow angle profiles.

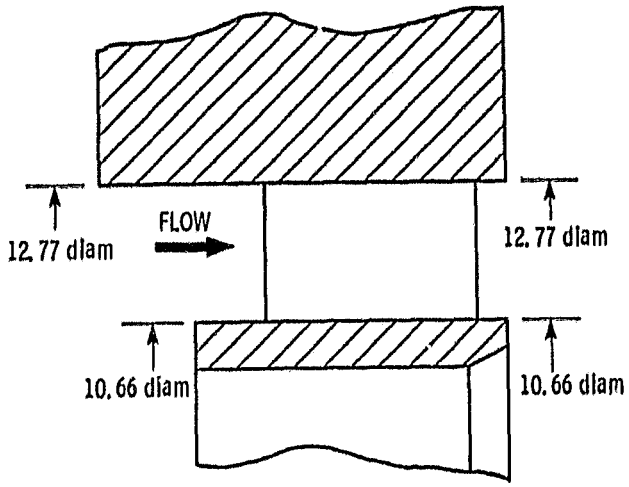

(a) Cylindrical stator.

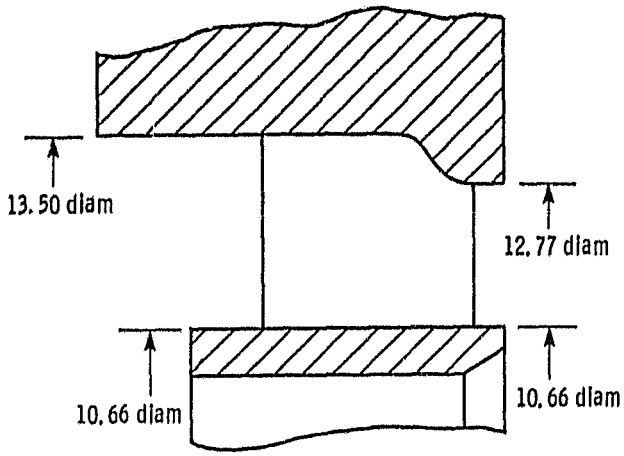

(b) Contoured stator A.

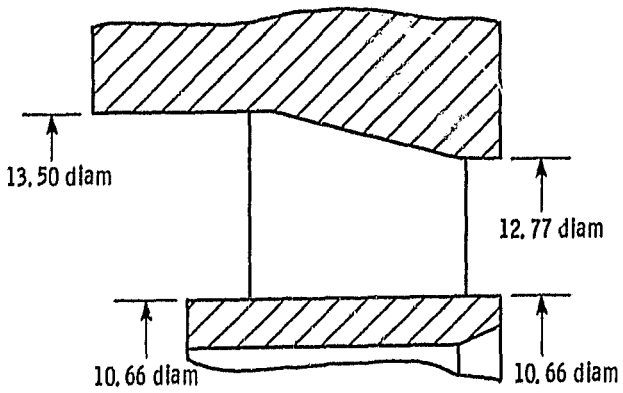

(c) Contoured stator B.

Figure 15. - Schematic cross-sectional view of three stator configurations tested. (Dimensions are in centimeters.)

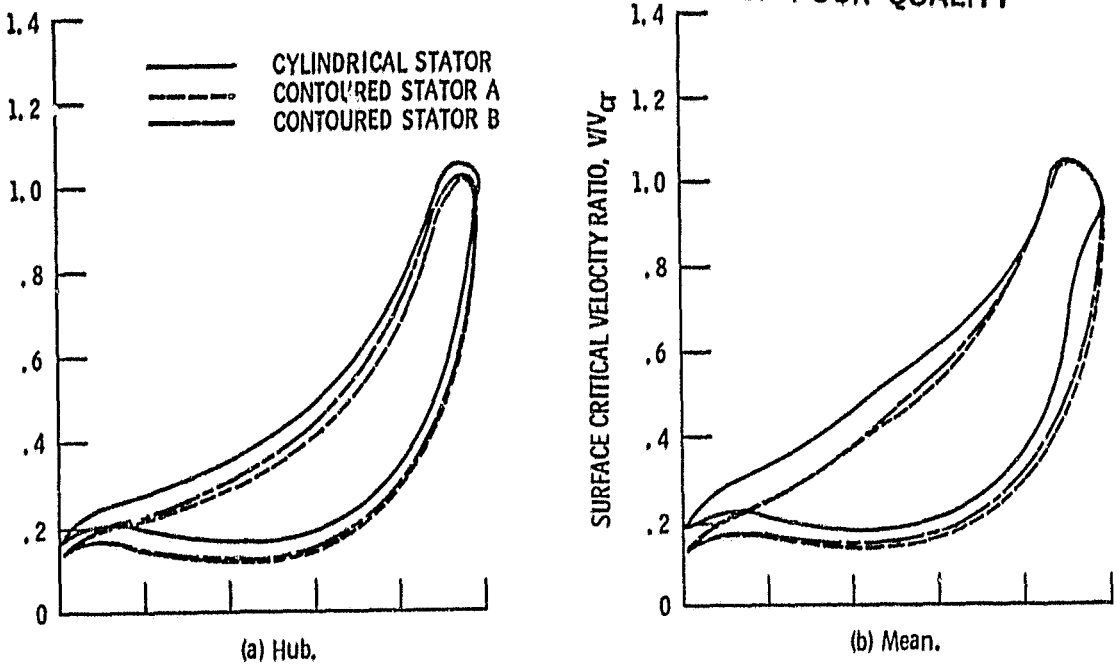

(a) Hub.

(b) Mean.

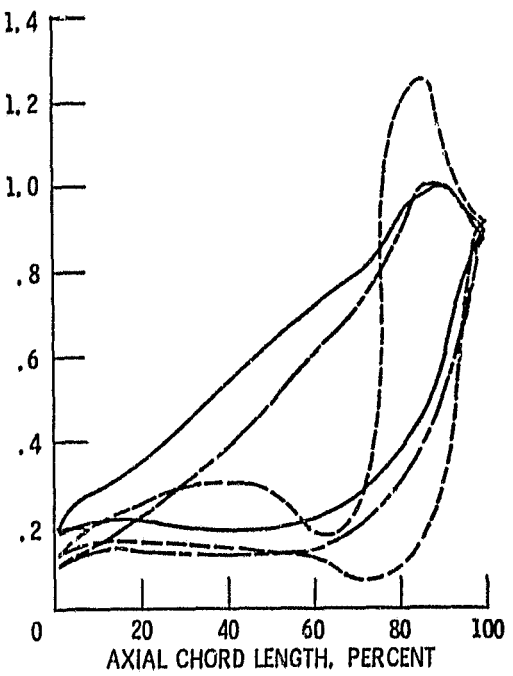

(a) Tip.

Figure 16. - Design blade surface velocity distributions for the three stator configurations.

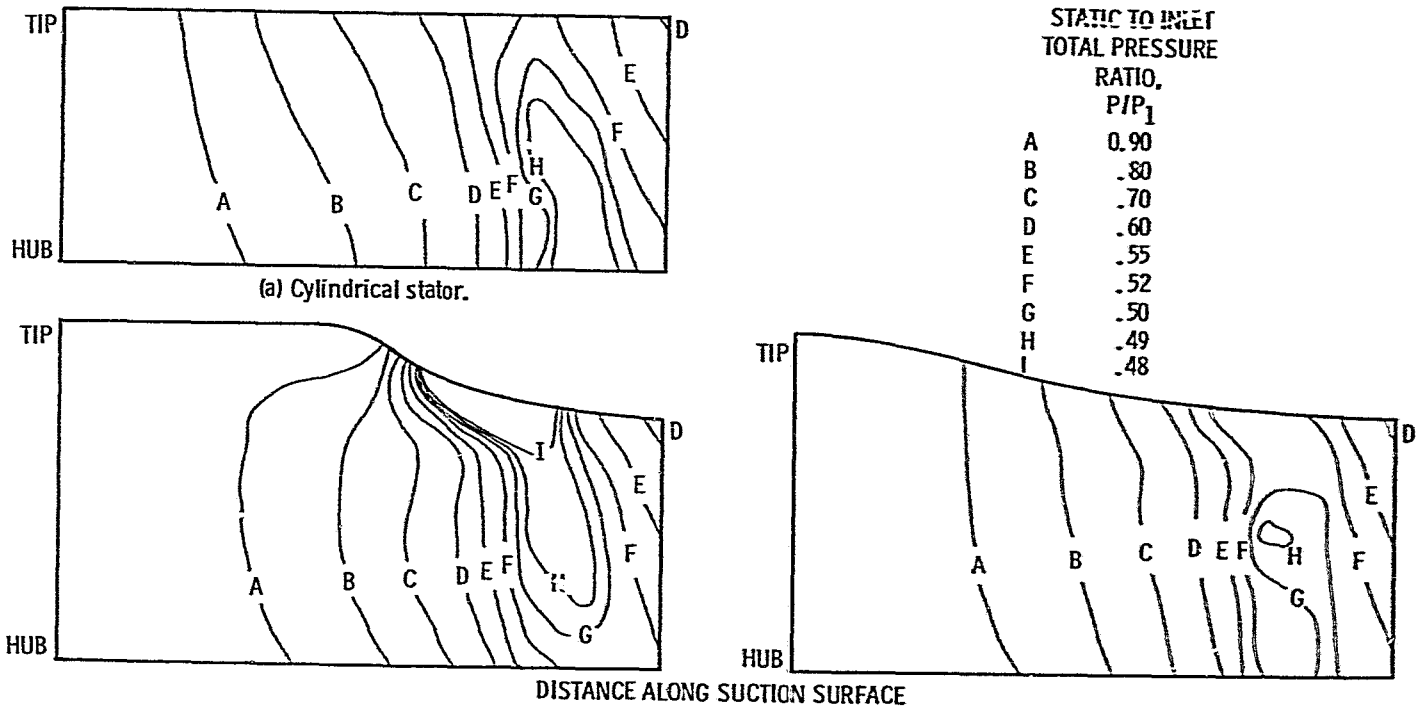

(a) Cylindrical stator.

(b) Contoured stator A.

(c) Contoured stator B.

Figure 17. – Comparison of analytical pressure distributions along suction surfaces of the three stator configurations.

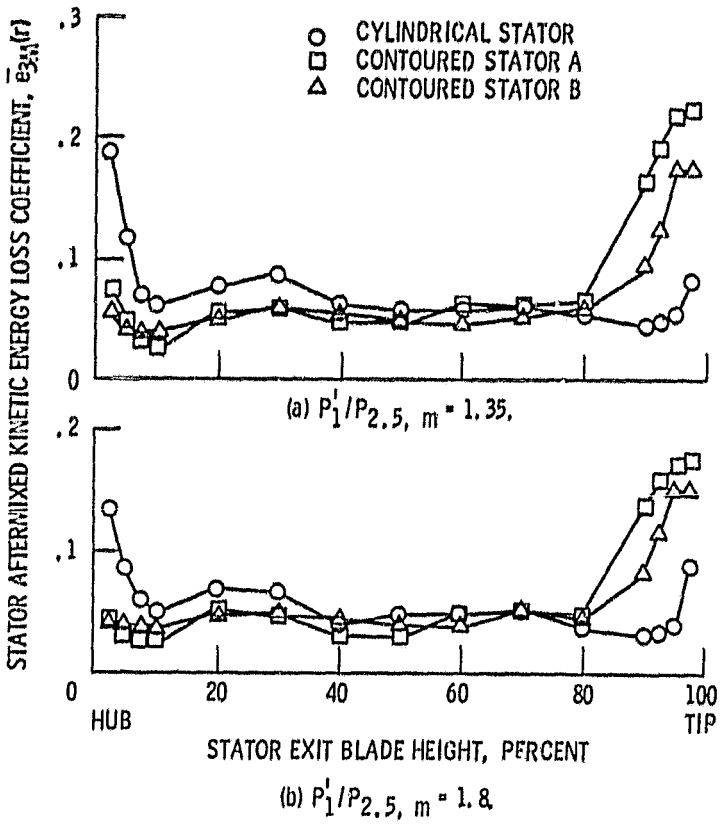

Figure 18. - Radial variation of stator kinetic energy loss coefficient.